PROCEEDINGS OF SCIENCE

# Development of the Matrix Element Method at Next-to-Leading Order for the Measurement of the Higgs Self-Coupling $\lambda_{3H}$

**Matthias Tartarin**[a,*] **and Jan Stark**[a]

[a] *Université de Toulouse, CNRS/IN2P3, L2IT, Toulouse, France*

*E-mail:* matthias.tartarin@l2it.in2p3.fr, jan.stark@l2it.in2p3.fr

The determination of the Higgs boson trilinear self-coupling $\lambda_{3H}$ is a key goal of the LHC physics programme. Its precise measurement will provide unique insight into the shape of the scalar potential and the mechanism of electroweak symmetry breaking. Higgs boson pair production in the $gg \to HH$ process, particularly in the $HH \to b\bar{b}\gamma\gamma$ final state, offers direct sensitivity to $\lambda_{3H}$. We present the first implementation of the Matrix Element Method at Next-to-Leading Order (MEM@NLO) for this channel. The MEM is a statistically optimal approach that maximises information extraction from collision events. Extending it to NLO represents a major methodological challenge, which we address with a new formalism integrated into the MoMEMta framework. Results with simulated pseudo-datasets demonstrate the strong discriminating power of the method and its ability to extract the coupling modifier $\kappa_\lambda = \lambda_{3H}/\lambda_{3H}^{SM}$ with high precision.

*The European Physical Society Conference on High Energy Physics (EPS-HEP2025)*
*7–11 July 2025*
*Marseille, France*

*Speaker



https://pos.sissa.it/

PoS(EPS-HEP2025)363

## 1. Introduction

The discovery of the Higgs boson in 2012 [1, 2] at the Large Hadron Collider (LHC) by the ATLAS [3] and CMS [4] collaborations completed the experimental confirmation of the Standard Model (SM) particle content, yet the form of the Higgs potential remains only weakly constrained. Its structure is probed through the trilinear Higgs self-coupling $\lambda_{3H}$, often expressed via the modifier $\kappa_\lambda = \lambda_{3H}/\lambda_{3H}^{\mathrm{SM}}$, which has a strong impact on both the rate and kinematics of Higgs boson pair production. Despite extensive searches, di-Higgs production has not yet been observed at the LHC, and the current limits on $\lambda_{3H}$ still allow sizeable deviations from the SM prediction. Using the full Run 2 dataset, ATLAS and CMS have performed combined interpretations of the major di-Higgs channels, yielding constraints of $-1.2 < \kappa_\lambda < 7.2$ at 95% CL for ATLAS [5] and $-1.4 < \kappa_\lambda < 7.0$ for CMS [6]. Further improvement requires analysis techniques capable of extracting the maximal discriminating power from event-level kinematics. The Matrix Element Method (MEM) offers such a framework. However, existing applications mostly rely on Leading-Order (LO) matrix elements, neglecting QCD radiation, and therefore suffer from reduced accuracy when applied to realistic LHC events. Several different approaches have been proposed to incorporate next-to-leading order (NLO) QCD effects within MEM-based analyses [7–10]. The strategy presented in this work introduces a new framework and realises the first MEM at Next-to-Leading Order (NLO) [11] for the process $gg \to HH \to b\bar{b}\gamma\gamma$, enabling a more precise and robust extraction of $\kappa_\lambda$ for realistic events. This study follows up on the results at LO only reported in Ref. [12].

## 2. The Matrix Element Method

The Matrix Element Method (MEM) was introduced in Refs. [13, 14] and later applied successfully in Refs. [15–17]. It provides a statistically optimal way to exploit the full kinematic information from collisions, by evaluating the likelihood that a measured event with reconstructed observables $\mathbf{x}^i$ originates from a given process $p$ under a set of model hypotheses $\mathbf{h}$. Each process corresponds to a specific hard-scattering topology, and is characterised by parameters $\mathbf{h}$ such as the coupling modifier $\kappa_\lambda$. The relevant signal process for this analysis is gluon-fusion di-Higgs production, $gg \to HH \to b\bar{b}\gamma\gamma$, while the main background processes include $t\bar{t}H$, QCD-induced diphoton production, and single-Higgs-plus-jets production.
For a given event $i$, the reconstructed quantities $\mathbf{x}^i$ represent the four-momenta of the reconstructed final-state objects, while the MEM integrates over all possible parton-level four-momenta $\mathbf{y}$ consistent with these measurements. From first principles, the process likelihood for a given event $i$ can be expressed as:

$$
\begin{aligned}
\mathcal{L}^{\mathrm{p}}_{\mathrm{process}}(\mathbf{h}|\mathbf{x}^i) &= \frac{d\sigma_p(pp \to \mathbf{x}^i; \mathbf{h}, W)}{\sigma_p^{\mathrm{obs}}(pp \to F)} \\
&= \frac{(2\pi)^4}{\sigma_p^{\mathrm{obs}}(pp \to F)} \int_{\mathbf{y}}\int_{q_1,q_2} \sum_{a_1,a_2} f_{a_1}(q_1) f_{a_2}(q_2) \frac{\left|\mathcal{M}_p(a_1 a_2 \to \mathbf{y}; \mathbf{h})\right|^2}{q_1 q_2 s} \\
&\quad \times W(\mathbf{y}, \mathbf{x}^i)\, \delta\Big(a_1 + a_2 - \sum_{j=1}^{n} y_j\Big)\, dq_1\, dq_2\, d^{4n}\mathbf{y},
\end{aligned} \tag{1}
$$

where:

- $\sigma_p^{\text{obs}}(pp \to F)$ denotes the observed integrated cross-section to produce the final state partons $F$,
- $q_1$ and $q_2$ are the momentum fractions of partons $a_1$ and $a_2$ (also referred to as Bjorken-$x$ scaling variables), and $s$ the Mandelstam variable corresponding to the squared centre-of-mass energy of the proton-proton collision,
- $\mathcal{M}_p(a_1 a_2 \to \mathbf{y}; \mathbf{h})$ is the Matrix Element of $a_1 a_2 \to \mathbf{y}$ for the process $p$ and the hypothesis $\mathbf{h}$, obtained from first principles,
- $\delta\Big(a_1 + a_2 - \sum_{j=1}^{n} y_j\Big)$ represents the energy-momentum conservation,
- $W(\mathbf{y}, \mathbf{x}^i)$ corresponds to the transfer functions, which parameterise the detector response and describe the probability for a parton-level configuration $\mathbf{y}$ to give rise to the reconstructed observables $\mathbf{x}^i$.

MoMEMta [18] is a modular framework designed to implement the MEM in high-energy physics analyses through numerical evaluation of the integral in Eq. (1). It provides a flexible environment in which the ingredients of the MEM integrand are defined and handled as separate *modules*. Yet because the MEM involves integrations over a high-dimensional phase space, the numerical complexity can quickly become very challenging. To make these complex calculations manageable, MoMEMta uses dedicated modules called *blocks* that perform analytic changes of variables using kinematic constraints (*e.g.* intermediate resonances) and conservation laws from the $\delta$-functions to reduce the initial dimensionality of the integration.
At LO, the MoMEMta modular approach performs remarkably well, as the phase space has a simple structure and the mapping between partonic and reconstructed objects is straightforward. At NLO however, additional complications arise. While virtual corrections preserve the LO final-state topology, real-emission contributions introduce an extra parton and therefore a different phase space. For this analysis however, the extra radiation will be treated as unresolved (*i.e.* no attempt is made to reconstruct the additional parton in the detector) and will be fully integrated over.

### 2.1 Accessing the Matrix Elements at NLO

Computing the likelihood $\mathcal{L}^{\text{p}}_{\text{process}}(\mathbf{h}|\mathbf{x}^i)$ requires access to the matrix element $\mathcal{M}_p$, evaluated at specific phase-space points. At NLO, this involves going beyond the leading Born term by including both virtual loop corrections and real-emission contributions. To obtain pointwise access to the amplitudes at arbitrary phase-space points, we use POWHEG-BOX-V2 [19], and in particular its dedicated ggHH subrepository developed by Heinrich *et al.* [20, 21]. POWHEG-BOX-V2 is a general NLO Monte Carlo framework designed for the computation of cross sections and the generation of fully exclusive events at NLO accuracy (with subsequent parton-showering provided via its interface to PYTHIA [22]), but is however not designed to provide direct access to matrix elements at arbitrary, user-defined phase-space points. A central part of this framework was to adapt POWHEG-BOX-V2 internal routines and to develop a dedicated interface to MoMEMta.

### 2.2 Design of the new Block N

The MoMEMta framework, originally designed for LO implementations of the MEM, does not include any block capable of handling the integration of real NLO contributions. To overcome this limitation, we developed a new component, Block N, specifically designed to incorporate the additional degrees of freedom related to real-emission contributions at NLO. The design principle of this new Block N is to simultaneously eliminate the two Bjorken-$x$ fractions ($q_1$, $q_2$) and the transverse components of the radiated parton momentum ($p_x^{\mathrm{rad}}$, $p_y^{\mathrm{rad}}$) using four-momentum conservation, while keeping its longitudinal component $p_z^{\mathrm{rad}}$ as a free integration variable.

### 2.3 Infrared safety and stability

A well-known feature of QCD perturbative calculations at fixed order are singularities in the soft and collinear limits for real emission matrix elements. These infrared singularities cancel against the corresponding virtual contributions once the full cross section is constructed. We modified POWHEG-BOX-V2 to provide the finite, infrared-safe Born+virtual and real-emission matrix elements at each phase-space point. When embedding these ingredients into the MEM, additional care is nevertheless required. To ensure stable and efficient numerical integration, two complementary technical measures were introduced. First, a dedicated collinear-treatment module to regulate configurations in which the additional parton becomes nearly parallel to an initial-state gluon or to one of the Higgs decay products. Second, a minimal transverse-momentum threshold on the radiated parton in the MEM integration, introduced solely to stabilise numerical convergence.

## 3. Validation and Discrimination Power

The most direct way to illustrate the discriminating power of the MEM@NLO is through rejection curves (ROC). For this analysis, it can be built from the ratio of likelihoods between the signal hypothesis and a given background process. By varying the cut placed on the likelihood ratio discriminant, one obtains the trade-off between signal and background efficiency. The comparison in Fig. 1 highlights the necessity of extending the MEM to NLO accuracy. When applied to realistic NLO-generated samples the MEM@LO exhibits a poor discrimination power, as it does not account for additional QCD radiation. In contrast, the MEM@NLO achieves a robust and stable discrimination power on NLO events.

## 4. Extraction of the Higgs Self-Coupling using likelihood scans

Beyond discrimination between the different processes $p$, the ultimate goal of the MEM@NLO is the extraction of the Higgs trilinear coupling modifier $\kappa_\lambda$. For that purpose one can define:

- The *kinematic likelihood* $\mathcal{L}_{\mathrm{kin}}(\kappa_\lambda)$, defined as the product of the per-event MEM likelihoods, each obtained from Eq. (1) as a weighted sum over all contributing processes. It captures the full kinematic information carried by the selected event sample.
- The *yield likelihood* $\mathcal{L}_{\mathrm{yield}}(\kappa_\lambda)$, exploits the strong dependence of the $gg \to HH$ production rate on $\kappa_\lambda$ which is known to vary quadratically due to the interference of the triangle and

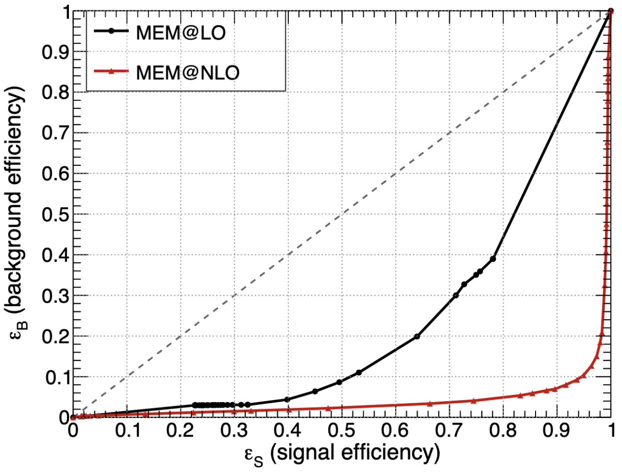


**Figure 1:** ROC curve for events generated at NLO, between the $ggF$ di-Higgs signal and ttH background. The black curve corresponds to MEM@LO, and the red curve to MEM@NLO. Given our conventions, the closer the ROC curve lies to the bottom-right corner of the plot, the more powerful the method.

box diagrams. This likelihood follows a Poisson distribution to observe $N_{\mathrm{obs}}$ events:

$$\mathcal{L}_{\mathrm{yield}}(\kappa_\lambda) = \frac{\mu(\kappa_\lambda)^{N_{\mathrm{obs}}} e^{-\mu(\kappa_\lambda)}}{N_{\mathrm{obs}}!}, \quad \text{with parameter } \mu(\kappa_\lambda) = N_{\mathrm{sig}}(\kappa_\lambda) + N_{\mathrm{bkg}}. \tag{2}$$

- The *extended likelihood* $\mathcal{L}_{\mathrm{ext}}$, defined as the product of the previous two, fully exploits both the kinematic and yield information.

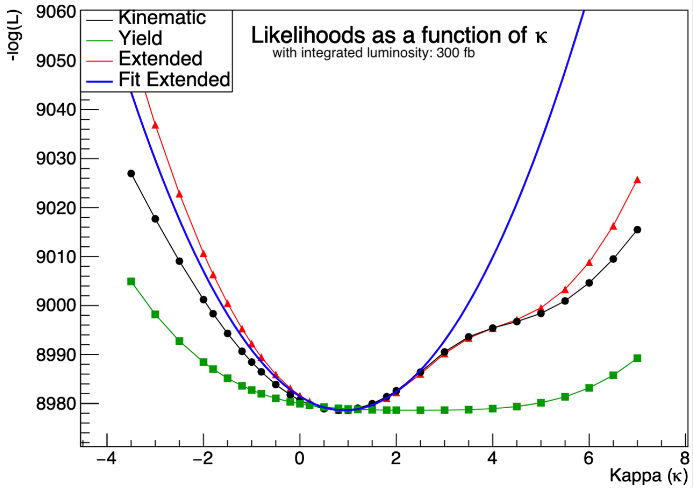


**Figure 2:** Likelihood scan for one pseudo–dataset consisting of a combination of NLO signal events ($\kappa_\lambda = 1.00$) and all main backgrounds, analysed using MEM@NLO. The graph shows $-\log\mathcal{L}$ as a function of the hypothesis $\kappa_\lambda$. **Black:** kinematic component ($\mathcal{L}_{\mathrm{Kin}}$) with offset; **Green:** yield term ($\mathcal{L}_{\mathrm{yield}}$) with offset; **Red:** extended likelihood ($\mathcal{L}_{\mathrm{ext}}$); **Blue:** quadratic fit to $-\log\mathcal{L}_{\mathrm{ext}}$ around its minimum, to extract the best–fit value $\hat{\kappa_\lambda}$ and an estimation on the associated uncertainty $\sigma_{\mathrm{measured}}$.

To quantify the performance, we generated 84 pseudo-datasets at NLO for an integrated luminosity of 300 fb$^{-1}$ per dataset, and with $\kappa_\lambda = 1$. The minimum of the profile of $-\log\mathcal{L}_{\mathrm{ext}}(\kappa_\lambda)$

determines the best-fit value $\hat{\kappa}_\lambda$, while the curvature around it provides information about the per-dataset statistical uncertainty (cf. Fig. 2). Repeating this procedure for large ensembles of pseudo-datasets allows one to build distributions of $\hat{\kappa}_\lambda$ and to assess both bias and resolution as shown in Fig. 3.

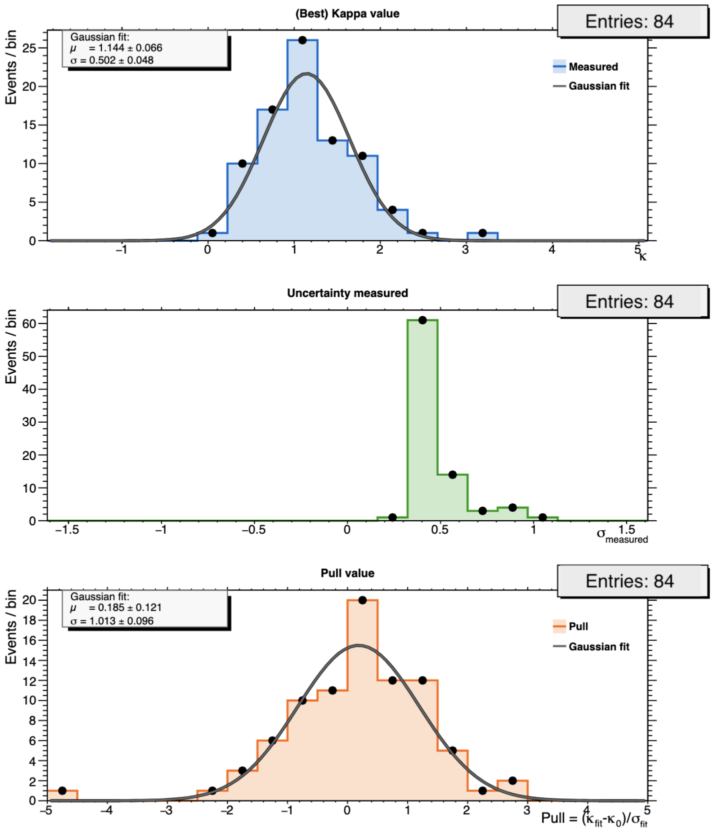


**Figure 3:** Histograms of likelihood scan results with all main backgrounds included. Top: distribution of the best-fit coupling parameter $\hat{\kappa_\lambda}$. Middle: distribution of the estimated uncertainty $\sigma_{\text{measured}}$. Bottom: distribution of the "pull" values $\omega$, defined as $(\hat{\kappa_\lambda} - \kappa_{\text{true}})/\sigma_{\text{measured}}$.

## 5. Results

To assess the performance of the MEM@NLO, we produce and analyse multiple samples with different background compositions. The results are summarised in Fig. 4. For each of the different configurations presented, the injected SM value $\kappa_\lambda = 1$ is always recovered, and well within uncertainties. The analysis of 84 pseudo-datasets, including **all main** backgrounds, yields $\kappa_\lambda = 1.144 \pm 0.502$ where 1.144 represents the mean over all pseudo-datasets, and 0.502 the expected 1-$\sigma$ uncertainty at 300 fb$^{-1}$. This result demonstrates that the MEM@NLO retains strong sensitivity, even in a challenging background-dominated environment. Another important result is that by exploiting the full event kinematics, the MEM@NLO excludes the mirror solution near $\kappa_\lambda = 4$, which arises in yield-based analyses because the inclusive $gg \to HH$ cross section depends only on the interference pattern between the triangle and box diagrams, leading to a second value of $\kappa_\lambda$ that reproduces the same total rate as the SM.



PoS(EPS-HEP2025)363

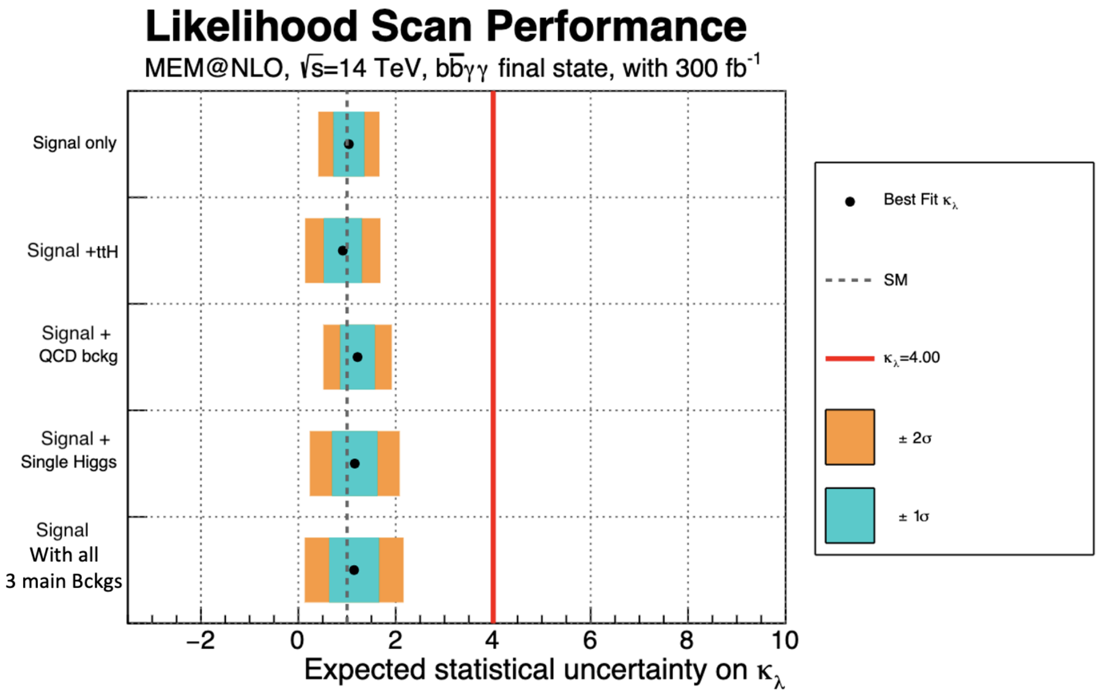


**Figure 4:** Summary of likelihood scan performance for MEM@NLO on NLO events generated with $\kappa_\lambda = 1$, in the $b\bar{b}\gamma\gamma$ final state, at $\sqrt{s} = 14$ TeV with 300 fb$^{-1}$. The black dot marks the mean best-fit value of $\kappa_\lambda$ for each ensemble of pseudo-datasets, while the bands show the expected $\pm 1\sigma$ (turquoise) and $\pm 2\sigma$ (orange) ranges. The dashed grey line is the SM prediction, and the red vertical line is the mirror solution at $\kappa_\lambda = 4$.

## 6. Conclusions and Outlook

We present the first implementation of MEM@NLO for Higgs boson pair production in the $b\bar{b}\gamma\gamma$ channel. A central achievement of this work is the development of Block N, a new integration block specifically engineered to treat the additional degrees of freedom associated with real-emission contributions at NLO. Its construction required a substantial extension of the existing MoMEMta formalism, enabling for the first time a consistent NLO treatment, resolving the limitations of previous LO-based approaches. Validation on simulated samples demonstrates significant improvements in discrimination power and parameter extraction. Ensemble tests confirmed the robustness of the method, and its ability to break the mirror solution degeneracy at $\kappa_\lambda = 4.0$. The method provides a powerful framework for extracting the Higgs self-coupling, and can be naturally extended to other analyses or processes. Future development of this work could focus on improving computational performance, refining the modeling of detector transfer functions, and exploring the application of MEM@NLO to a broader range of final states (*e.g.* $b\bar{b}\tau^+\tau^-$ or $b\bar{b}b\bar{b}$).

## Acknowledgments

We gratefully acknowledge the support of our colleagues at the **IN2P3 Computing Centre** (CC-IN2P3) in Lyon (Villeurbanne) for the reliable and efficient operation of their computing farms. Without this facility, the present study would not have been possible.

## References

[1] ATLAS Collaboration, *Observation of a new particle in the search for the Standard Model Higgs boson with the ATLAS detector at the LHC*, *Physics Letters B* **716** (2012) 1–29, doi: 10.1016/j.physletb.2012.08.020.

[2] CMS Collaboration, *Observation of a new boson at a mass of 125 GeV with the CMS experiment at the LHC*, *Physics Letters B* **716** (2012) 30–61, doi: 10.1016/j.physletb.2012.08.021.

[3] The ATLAS Collaboration, *The ATLAS Experiment at the CERN Large Hadron Collider*, *Journal of Instrumentation* **3** (2008), doi: 10.1088/1748-0221/3/08/S08003.

[4] The CMS Collaboration, *The CMS Experiment at the CERN LHC*, *Journal of Instrumentation* **3** (2008), doi: 10.1088/1748-0221/3/08/S08004.

[5] ATLAS Collaboration, *Combination of searches for Higgs boson pair production in $pp$ collisions at $\sqrt{s}$ = 13 TeV with the ATLAS detector*, *Phys. Rev. Lett.* **133**, 101801 (2024), doi: 10.1103/PhysRevLett.133.101801.

[6] CMS Collaboration, *Combination of searches for nonresonant Higgs boson pair production in proton–proton collisions at $\sqrt{s}$ = 13 TeV*, submitted to Reports on Progress in Physics, arXiv: 2510.07527 (2025).

[7] T. Martini and P. Uwer, *Extending the Matrix Element Method beyond the Born approximation: calculating event weights at next-to-leading order accuracy*, *JHEP* **09**, 083 (2015), doi:10.1007/JHEP09(2015)083.

[8] T. Martini and P. Uwer, *The Matrix Element Method at next-to-leading order QCD for hadronic collisions: single top-quark production at the LHC as an example application*, *JHEP* **05**, 141 (2018), doi:10.1007/JHEP05(2018)141.

[9] M. Kraus, T. Martini and P. Uwer, *Matrix element method at NLO for (anti-)$k_t$-jet algorithms*, *Phys. Rev. D* **100**, 076010 (2019), doi:10.1103/PhysRevD.100.076010.

[10] T. Martini, T. Nuraliyev and P. Uwer, *Determination of the top-quark mass from top-quark pair events with the matrix element method at next-to-leading order: Potential and prospects*, https://arxiv.org/abs/2301.03280 [hep-ph] (2023) .

[11] M. Tartarin, *Measurement of the Higgs self-coupling using the Matrix Element Method at Next-to-Leading Order (NLO) in the $gg \to HH \to b\bar{b}\gamma\gamma$ channel for the ATLAS experiment at the LHC*, Ph.D. thesis, Université de Toulouse, (2025), doi: 10.17181/8hbdr-mgg27.

[12] F. Eble and J. Stark, *Prospective study for the development of an analysis to measure the tri-linear Higgs coupling using the Matrix Element Method with the ATLAS experiment at the HL-LHC*, Master thesis, KTH Royal Institute of Technology (2020), `https://urn.kb.se/resolve?urn=urn:nbn:se:kth:diva-291100`.



PoS(EPS-HEP2025)363

[13] K. Kondo, *Dynamical Likelihood Method for Reconstruction of Events with Missing Momentum. I. Method and Toy Models*, *J. Phys. Soc. Jap.* **57**, no. 12, 4126–4140 (1988), doi: 10.1143/JPSJ.57.4126.

[14] K. Kondo, *Dynamical Likelihood Method for Reconstruction of Events with Missing Momentum. II. Mass Spectra for* $2 \to 2$ *Processes*, *J. Phys. Soc. Jap.* **60**, no. 3, 836–844 (1991), doi: 10.1143/JPSJ.60.836.

[15] DØ Collaboration, *Measurement of the Top Quark Mass Using Dilepton Events*, *Phys. Rev. Lett.* **80**, 2063–2068 (1998), doi: 10.1103/PhysRevLett.80.2063, arXiv: 9706014.

[16] F. Canelli, *Helicity of the W boson in single-lepton $t\bar{t}$ events*, Ph.D. thesis, Rochester University (2003), doi: 10.1142/S0217751X03016689.

[17] DØ Collaboration, *A Precision Measurement of the Mass of the Top Quark, Nature* **429**, 638 (2004), doi: 10.1038/nature02589, arXiv: 0406031.

[18] S. Wertz et al., *MoMEMta, a modular toolkit for the Matrix Element Method at the LHC*, *Eur. Phys. J. C* **79**, 2 (2019), doi: 10.1140/epjc/s10052-019-6635-5.

[19] S. Alioli, P. Nason, C. Oleari and E. Re, *A general framework for implementing NLO calculations in shower Monte Carlo programs: the POWHEG BOX*, *J. High Energ. Phys.* **2010** (6), 43 (2010), doi: 10.1007/JHEP06(2010)043.

[20] G. Heinrich et al., *NLO predictions for Higgs boson pair production with full top quark mass dependence matched to parton showers*, *JHEP* **08**, 088 (2017), doi: 10.1007/JHEP08(2017)088, arXiv: 1703.09252.

[21] G. Heinrich et al., *Probing the trilinear Higgs boson coupling in di-Higgs production at NLO QCD including parton shower effects*, *JHEP* **06**, 066 (2019), doi: 10.1007/JHEP06(2019)066, arXiv: 1903.08137.

[22] T. Sjöstrand et al., *An Introduction to PYTHIA 8.2*, *Comput. Phys. Commun.* **191**, 159–177 (2015), doi: 10.1016/j.cpc.2015.01.024, arXiv: 1410.3012.

PoS(EPS-HEP2025)363